Stellar Coronae in the Chandra and XMM-Newton Era
ASP Conference Series, Vol. TBD, 2001
F. Favata & J. Drake

The Solar Atmosphere at Radio Wavelengths

Stephen M. White

Department of Astronomy, University of Maryland, College Park, MD 20742, USA

Abstract. We briefly review the status of radio observations of the solar atmosphere with an emphasis on relevance to stellar observations.

1. Radio Emission Mechanisms

Solar radio observations are sensitive to virtually every feature of the solar atmosphere, covering a temperature range from the temperature minimum (5000 K) up to the soft X-ray-emitting plasma produced by solar flares ($> 10^7$ K) and the most energetic electrons accelerated by the Sun (energies > 1 MeV). The reason for this broad sensitivity lies in the fact that four very different emission mechanisms, each of them well understood, contribute to opacity at radio wavelengths: (i) free–free or bremsstrahlung emission is the ubiquitous mechanism of solar radio astronomy, present even when the others are absent. The opacity is proportional to $N_e N_i / f^2 T^{1.5}$ where N_e, N_i are the electron and ion number densities, f the frequency and T the temperature. It is therefore particularly effective at high densities, low frequencies and low temperatures. (ii) "H^- opacity" is the misnomer applied to the mechanism that replaces bremsstrahlung at the very low temperatures in the lower chromosphere at which H and He are neutral. Free electrons due to ionization of light metals such as sodium can polarize an H atom and the interaction between the electrons and the dipolar atoms provides opacity. This mechanism is responsible for the quiet–Sun contribution to radio emission at very high frequencies where the optically thick layer in the solar atmosphere lies low in the chromosphere or temperature minimum where the temperature is well below 10^4 K. (iii) Gyroresonance opacity is due to the acceleration experienced by an electron moving through a magnetic field under the Lorentz force. The acceleration associated with the gyromotion provides opacity in the radio regime at frequencies that are integer multiples (*harmonics*) of the electron gyrofrequency, $f_B = 2.8 \times 10^6 B$ Hz, where the magnetic field B is measured in gauss (G). This is the dominant source of opacity in regions of strong magnetic fields in the corona. The nonthermal version of gyroemission (called "gyrosynchrotron" emission when mildly relativistic electrons dominate, or "synchrotron" when ultrarelativistic electrons dominate) is responsible for most flare radio emission. (iv) Plasma emission is commonly found to be produced by energetic electrons at low frequencies. It involves the production of electrostatic Langmuir waves at the plasma frequency $f_p = 9000 \sqrt{N_e}$ (N_e measured in cm^{-3}), and the subsequent conversion of these electrostatic waves to propagating electromagnetic waves at f_p and its harmonics. This mechanism produces the well-known "zoo" of radio bursts at low frequencies where electron beams and shocks can radiate efficiently and free–free absorption is low.

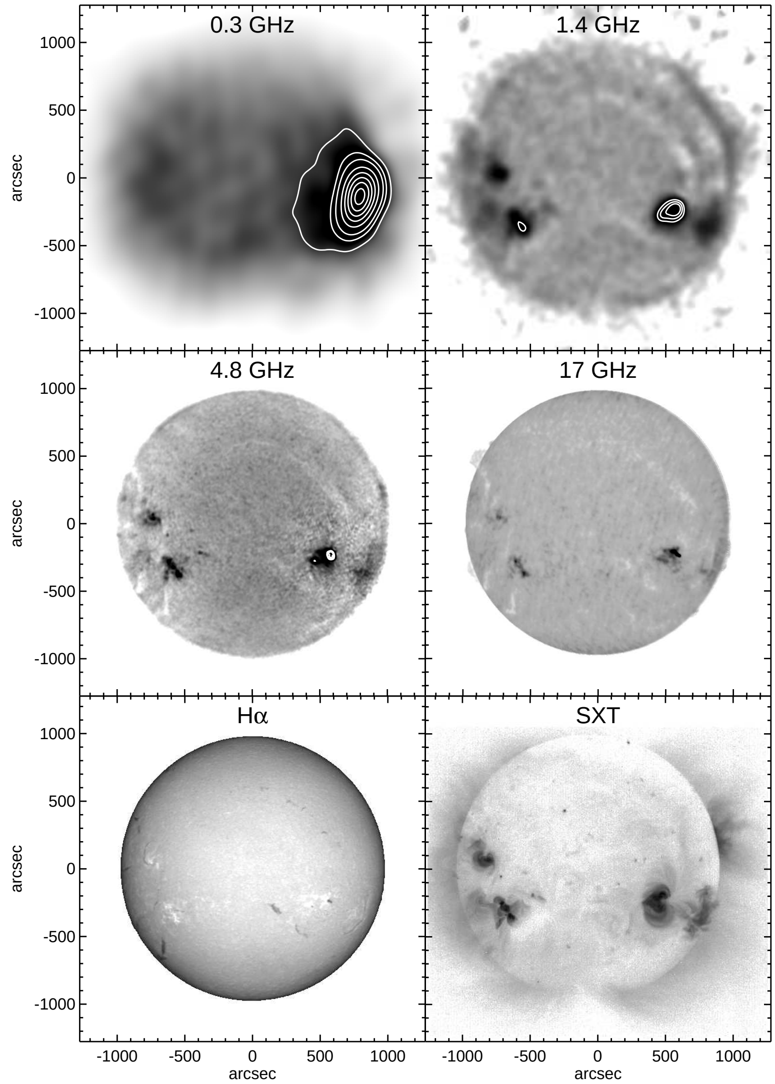

Figure 1. The changes in the appearance of the Sun as a function of radio frequency on 1993 November 7. The resolutions are 220″ at 0.3 GHz, 50″ at 1.4 GHz and 12″ at 4.8 GHz and 17 GHz. The 0.3, 1.4 and 4.8 GHz images were made with the Very Large Array radiotelescope, while the 17 GHz image is made with the Nobeyama Radioheliograph. White contours highlighting the brightest features are plotted at brightness temperatures of 0.8, 1.2, 1.6, 2.4, 3.2, 4.0, 4.8 and 5.6 $\times$ 10^6 K. The color table saturates (is black) at 0.8 $\times$ 10^6 K at 0.3 GHz, 0.6 $\times$ 10^6 K at 1.4 GHz, 0.1 $\times$ 10^6 K at 4.8 GHz and 0.022 $\times$ 10^6 K at 17 GHz. For comparison, Hα (Big Bear Solar Observatory) and soft X-ray (Yohkoh/SXT) images from the same day are also shown.

2. The Sun at Radio Wavelengths

The combination of emission mechanisms discussed above is responsible for the fact that radio images can look like a mixture of coronal and chromospheric images. Figure

1 shows radio images at four very different frequencies, together with Hα and soft X-ray images for comparison. Different frequencies penetrate to different depths in the solar atmosphere, depending on local conditions, so that the appearance of the Sun changes dramatically over the radio frequency range.

An important feature of solar radio emission is that every frequency becomes optically thick (i.e., opaque) at some point in the solar atmosphere. Just as we cannot see below the photosphere in visible light, in a radio image at a given frequency we cannot see material below the optically thick layer. Radio wavelengths lie in the Rayleigh–Jeans limit, $h\nu \ll kT$, and therefore the radio flux is proportional to the brightness temperature. In the optically thick layer the brightness temperature is equal to the local electron temperature so that (unlike most other diagnostics of the solar atmosphere) radio images can often be interpreted directly as temperature maps. Since temperature in the solar atmosphere generally increases outwards from the temperature minimum (just above the photosphere), it is also possible for a radio image to show both the emission from the low–lying cooler optically–thick layer as well as contributions from hotter optically–thin plasma in the overlying atmosphere.

As noted above, free–free opacity increases rapidly as frequency decreases and it dominates the quiet radio Sun at low frequencies. The whole solar corona is optically thick at frequencies below 500 MHz, so that the Sun appears as a large relatively featureless source with a dimension larger than the solar radius, usually elongated in the equatorial direction due to the fact that the solar atmosphere is generally of higher density at the equator than at the poles. Since the whole corona is at a temperature of order $1 - 2 \times 10^6$ K, there is little contrast between quiet features on the solar disk at low frequencies. As is often the case at low frequencies, the brightest radio feature in the 0.3 GHz image shown (the feature at the right edge of the 0.3 GHz disk) is not due to free–free opacity at all, but rather is a form of broadband coherent emission called a noise storm, commonly found over very active regions in the frequency range 200–500 MHz.

As frequency increases above 500 MHz the quiet solar atmosphere starts to become optically thin and its brightness temperature drops, while the enhanced density in the corona above active regions maintains a high optical depth and hence high brightness temperatures. Thus at 1.4 GHz radio images of the Sun show much more contrast between features, depending on their density. Virtually all the non–flaring radio emission seen at 1.4 GHz is believed to be produced by free–free emission. However, as frequency rises the layer that is optically thick due to free-free opacity drops rapidly in height, exposing the layers of constant magnetic field in the corona that are made optically thick by gyroresonance emission. Thus at 4.8 GHz the only sources that have coronal brightness temperatures (i.e., are optically thick in the corona) are gyroresonance sources over sunspots where the coronal magnetic field exceeds 600 G. The other bright features, such as those near the east limb, are due to optically–thin free–free emission from dense structures in the corona (these also show up prominently as bright sets of loops in X–ray images), and have brightness temperatures of order 10^5 K. Low–density features clearly show up as regions of reduced brightness, e.g., within the active–region complex near the east limb, and in the filament channel stretching across the north–west quadrant. The disk at this frequency is at a brightness temperature of order 20000 K, corresponding to the lower transition region/upper chromosphere. The radius of the radio disk at 4.8 GHz is of order $30''$ larger than the optical photosphere.

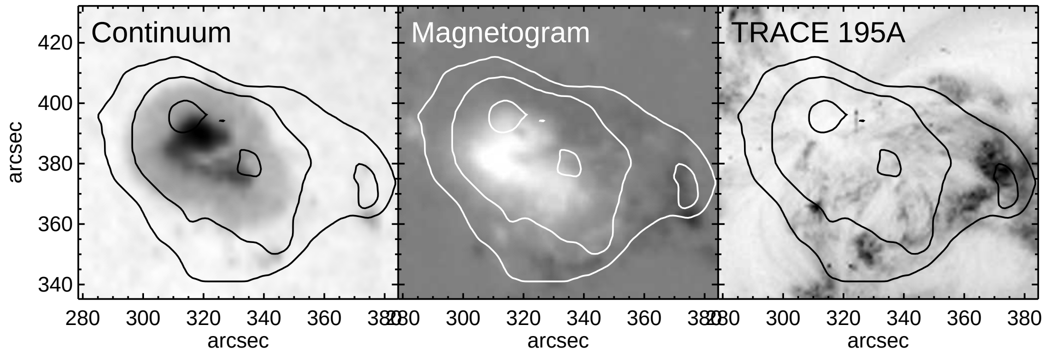

Figure 2. Contours of magnetic field strength at the base of the corona plotted on white light (left), magnetogram (middle) and TRACE 195 Å Fe XII (right) images of a sunspot observed on 1999 May 13. The coronal contours are plotted at 500, 900 and 1700 G, corresponding to the radio images at 4.5, 8.0 and 15.0 GHz used to construct the coronal magnetogram. Note the displacement of the 1700 G coronal magnetic field strength from the strongest photospheric fields, due in part to projection effects resulting from the height of the radio–emitting layer. Axes are labelled in arcseconds from apparent disk center.

At yet higher frequencies the optically thin contributions from hot dense coronal material diminish rapidly. Gyroresonance emission can continue to produce features with brightness temperatures in excess of 10^6 K as long as sufficiently strong magnetic fields are present in the corona. The upper limit to coronal magnetic field strengths is not known, but may be of order 3000 G, which could produce gyroresonance emission up to 25 GHz. Above the highest frequency at which gyroresonance emission is effective, there is no form of opacity available that can make coronal features optically thick and consequently the contrast between the disk and the brightest features in the radio image is greatly reduced. The height of the layer in which a given frequency becomes optically thick continues to drop through the chromosphere as frequency increases: the brightness temperature of the disk component is of order 6700 K at 100 GHz and 5800 K (corresponding to the vicinity of the temperature minimum) at 300 GHz, with contrasts only of order 10% being seen in the images.

3. Radio Observations of Coronal Magnetic Fields

One of the strengths of solar radio astronomy is its ability to measure coronal magnetic field strengths. Photospheric and chromospheric field strengths can be measured with optical and infrared lines, but presently no magnetically sensitive coronal lines have been identified that can be used to measure coronal magnetic fields against the bright solar disk. Such fields can easily be measured at radio wavelengths using gyroresonance emission. The properties of the emission mechanism are very well understood (e.g., Zlotnik 1968; White & Kundu 1997): (i) Opacity is only significant in narrow layers of constant magnetic field strength where the resonance condition $f = sf_B$ (s = 1, 2, 3, 4, ...) is satisfied. (ii) The two natural electromagnetic modes of the plasma are circularly polarized under most conditions: the x mode, which rotates in the same sense as the electron gyrates about the field, interacts more strongly than the o mode that has the opposite sense of rotation. The o mode opacity is always at least an order of magnitude smaller than the x mode opacity. The two modes are observed as opposite circular polarizations by a radio telescope. (iii) The gyroresonance opacity at harmonic s is $\propto N_e\,(s^2 \sin^2\theta\, T_e/m_e c^2)^{s-1}$, where θ is the angle between the line of sight and the magnetic field direction in the source, N_e the electron density and T_e is the temperature. The opacity drops sharply towards small θ (**B** parallel to the line of sight) in both modes. (iv) For typical coronal conditions, the x mode is optically thick ($\tau \geq 1$) in the $s = 2$ and 3 layers over a broad range of angles θ. The o mode is optically thick over most of the $s = 2$ layer, and may be at least marginally optically thick over a small portion of the $s = 3$ layer where θ is large. Harmonics greater than $s = 4$ do not have any significant optical depth in the quiet solar corona, although there may be x mode emission from the 4th harmonic if the temperature is high (Lee et al. 1997). (v) For each increase of s by 1, the opacity in a given mode at a given angle drops by slightly more than 2 orders of magnitude. This is largely due to the $(T_e/mc^2)^s$ dependence of the opacity. The importance of this large change in opacity from one layer to the next is that a given harmonic layer is likely to be either optically thick over a wide range of angles θ, or else optically thin everywhere. Density has much less influence on the opacity than the harmonic number. (vi) The thermal width of the cyclotron resonance at coronal temperatures is such that B typically varies by less than 2% across a resonant layer, corresponding to a physical width of less than 200 km for typical coronal magnetic gradients (scale length $\sim 10^4$ km).

When "decoding" observations of gyroresonance emission in terms of coronal magnetic fields, we can regard any source above 3 GHz that has a coronal brightness temperature or a high degree of circular polarization as a gyroresonance source (free-free does not have sufficient opacity at the higher frequencies to make the corona optically thick). It is helpful to think in terms of the surfaces of constant magnetic field strength ("isogauss") above an active region. At a given frequency f, gyroresonance opacity is only significant in the isogauss layers along the line of sight at which $f_B = f/s$, s = 1,2,3,... When we look down on an active region from above, we see down to the highest isogauss layer that is optically thick in the corona. This will generally be the $s = 3$ layer in the sense of circular polarization corresponding to the x mode and the $s = 2$ layer in the o mode, e.g., the 600 G layer in the x mode and 900 G in the o mode at 5 GHz. For a region on the disk θ, and therefore opacity, will be largest at the outer boundary of an isogauss layer: thus the outer boundary of the optically thick radio source should indicate where the isogauss surface drops below the corona into the chromosphere. This property allows us straightforwardly to measure the magnetic field strength at the base of the corona. An example of this diagnostic is shown in Figure 2. An important point is that gyroresonance observations are sensitive to the absolute magnetic field strength B, whereas conventional (Babcock or Leighton style) optical magnetographs measure only the line–of–sight component of the magnetic flux, $B\cos\theta \times$ *area*, and thus are of limited value for regions near the solar limb.

4. Solar Flares at Radio Wavelengths

Solar flares radiate strongly at radio wavelengths (Bastian, Benz & Gary 1998). They accelerate electrons to nonthermal energies, and such electrons tend to form beams that are subject to plasma instabilities capable of generating high brightness temperature

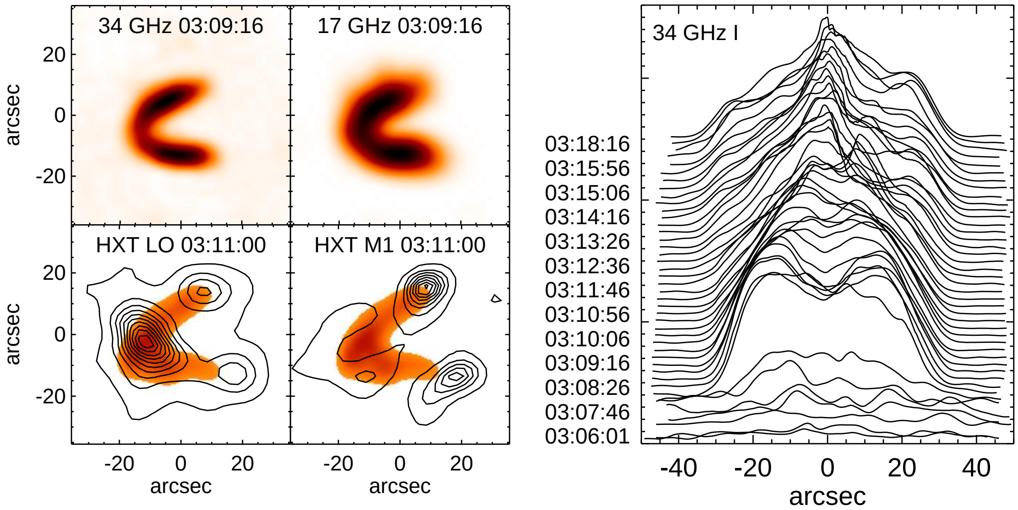

Figure 3. Observations of a flare loop on 1999 May 29. The images at left show (upper panels) radio images from NoRH at 34 GHz (resolution $6''$) and 17 GHz (resolution $9''$), together with (lower panels) contours of the hard X-ray emission (HXT data) in the LO channel (14-23 keV) and M1 channel (23-33 keV) superposed on a greyscale representation of the SXT soft X-ray image of the loop at 03:11:30 UT. The panel at right shows a time sequence of intensity profiles at 34 GHz measured along the spine of the loop, showing morphological evolution from having peaks at the two legs of the loop initially to having a bright looptop source as in the SXT image later in the event.

emissions at the plasma frequency and the electron gyrofrequency. These emissions are responsible for a range of radio bursts with peculiar spectral and temporal properties that are prominent at low radio frequencies (below 2 GHz); at higher frequencies such emissions are probably suppressed by strong thermal free-free damping in the surrounding medium. White & Franciosini (1995) argued that such emissions might be more prominent on active stars that have hotter coronae, so that the free-free damping rate at a given density ($\propto T^{-1.5}$) will be lower than on the Sun.

Electrons with energies above 100 keV also radiate very strongly by the gyrosynchrotron process whenever they are in coronal magnetic fields. Radio telescopes can thus be used to make high-resolution images of the sources of nonthermal electrons in solar flares. Figure 3 shows an example of such an image: this is a flare loop filled with nonthermal mildly relativistic electrons radiating gyrosynchrotron emission. The distribution of the emission pattern along the loop changes with time in this event: since we understand the mechanism, we can use resolved images such as this to model the magnetic structure of the loop and the properties of the radiating electrons (Nindos et al. 2000). In addition to bursts such as this one, in the low corona, gyrosynchrotron emission has now been imaged from the expanding front of a coronal mass ejection high in the corona (Bastian et al. 2001).

Solar flares also produce large volumes of heated thermal plasma, at least in part due to heating of chromospheric material to coronal temperatures by the nonthermal electrons accelerated in the flare energy release. This hot plasma can also be detected

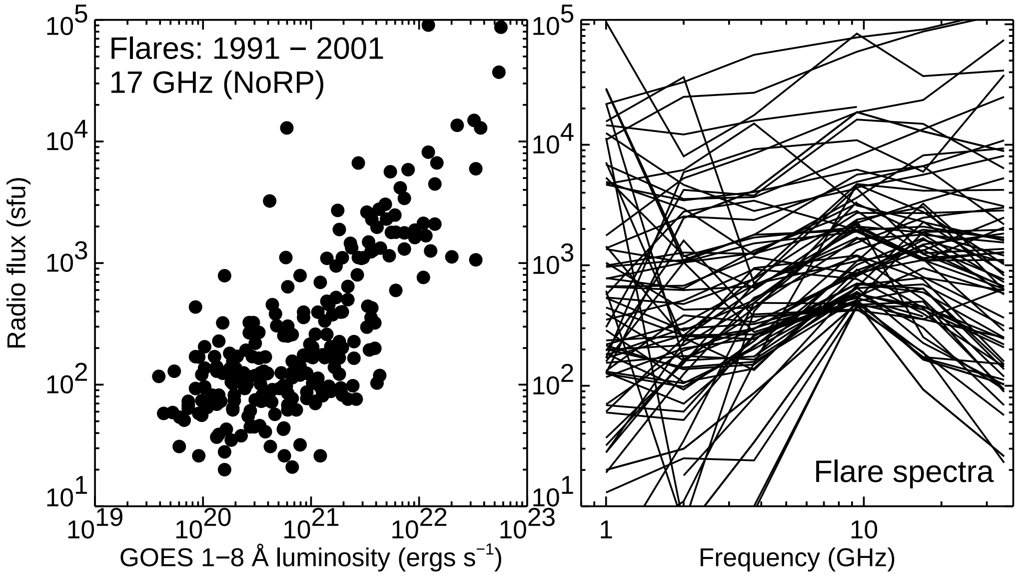

Figure 4. Data for the radio flux of flares. The left panel shows the correlation between the peak 17 GHz flux measured by the Nobeyama polarimeters and the corresponding peak soft X-ray flux in the GOES 1-8 Å band for 251 events from 1991 to 2001 on a log-log plot. The right panel shows the radio spectra of the same set of flares, i.e., for each event we plot the peak radio flux measured at 1, 2, 3.75, 9.4 and 17 GHz. This figure shows that while most events have a radio spectral peak around 10 GHz, a significant fraction, particularly amongst the larger events, has a spectral peak above 17 GHz.

at radio wavelengths because of its free-free emission, but it is usually weaker than the nonthermal emission produced in the impulsive phase of the flare and peaks much later. Despite this, there is a general correlation between the peak radio flux measured in a flare, which depends on the number of nonthermal electrons present and on a high power of the magnetic field strength in the source (typically $\propto B^2 - B^4$), and the peak soft X-ray flux, which depends largely on the total energy released in the flare. Figure 4 shows this relation for 251 events using radio fluxes at 17 GHz and GOES 1-8 Å soft X-ray measurements: loosely speaking the peak radio flux is proportional to the peak soft X-ray flux, with considerable spread, over 4 orders of magnitude. The radio emission detected from active stars is believed to be gyrosynchrotron emission from a population of non-flare nonthermal electrons occupying the stellar corona, and the quiescent soft X-ray emission from active stars has a component almost as hot as the soft X-ray emission of solar flares, so when we compare solar and stellar behaviour we might expect that we should be comparing quiescent stellar data with solar flare data, and indeed it turns out that stars show a relationship between their radio and X-ray fluxes that is very similar to that shown in Figure 4 for solar flares: $\log L_{radio} = \log L_{X-ray} - 15.5$ (Güdel et al. 1993; Benz & Güdel 1994). This relationship between nonthermal and thermal quantities is not easily explained (Güdel & Benz 1993; White 1996).

Figure 4 also shows the typical radio spectra of the nonthermal emission from solar flares. It is a remarkable fact that most solar flare radio spectra peak near 10

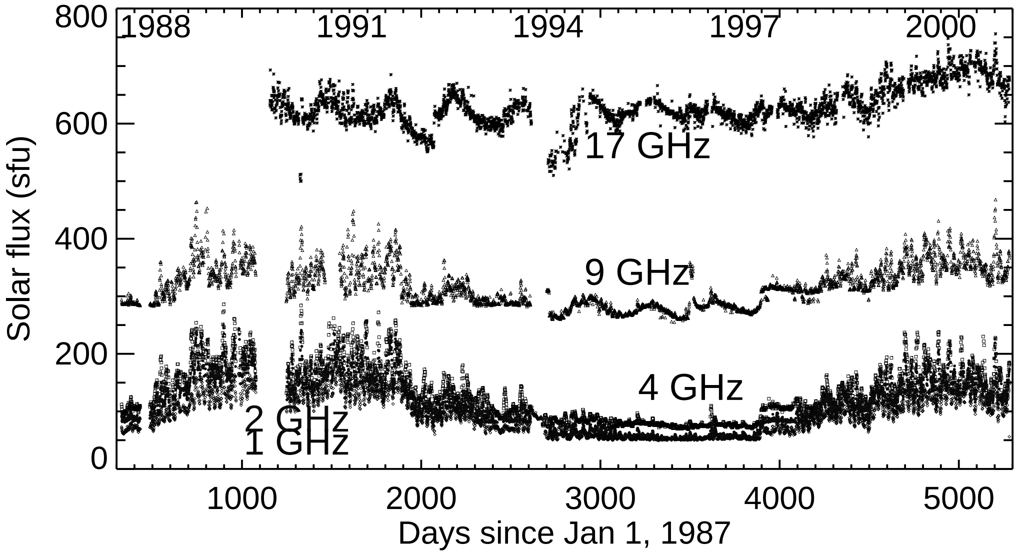

Figure 5. The solar cycle variation of the radio flux of the Sun measured at 5 different frequencies. The data are from the Nobeyama Radio Observatory polarimeters at 1, 2, 3.75, 9.4 and 17 GHz; fluxes at 1 GHz are less than those at 2 GHz but they are hard to distinguish on this plot.

GHz. Some flares do have higher spectral peaks, particularly large flares. For gyrosynchrotron emission the location of the peak in the radio spectrum is almost completely determined by the magnetic field strength in the radio source (being about $5f_B$: Dulk 1985). This implies that many solar flare radio sources lie in sources with magnetic field strengths of order 600 G. Why there should be such similarity in this parameter is not well understood.

5. Solar and Stellar Cycles at Radio Wavelengths

Measurements of activity cycles on other stars for comparison with the well-observed solar case is an important input for the study of solar and stellar dynamos, so it is relevant to investigate how the solar dynamo is revealed in radio observations. Figure 5 shows daily measurements of the variation of the solar radio flux over the solar cycle from the Nobeyama Radio Observatory polarimeters at 1, 2, 3.75, 9.4 and 17 GHz (Torii et al. 1979; Nakajima et al. 1985). Typical fluxes rise from 60 sfu (1 solar flux unit = 10^{-19} ergs s^{-1} cm^{-2} Hz^{-1}) at 1 GHz up to 600 sfu at 17 GHz. If the radio brightness temperature of the Sun were fixed then the flux would rise roughly as frequency squared: the observation that it does not is due to the fact that the optically thick layer in the solar atmosphere drops as frequency rises. In particular, at solar minimum the 2 GHz flux is only 10% larger than the 1 GHz flux because this is the frequency range in which the corona becomes optically thin and the brightness temperature drops from about 250000 K at 1 GHz to 60000 K at 2 GHz. At higher frequencies the effective temperature of the solar disk has a much weaker dependence on frequency and the f^2 dependence is mostly restored.

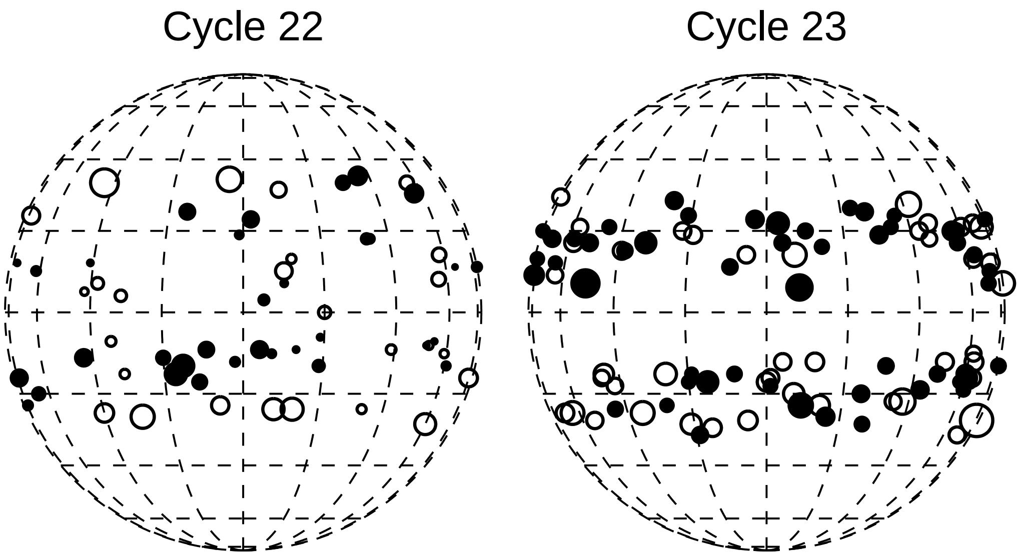

Figure 6. Measurements of the sense of circularly polarized flux from solar flares during two solar cycles. The radio measurements are from the 17 GHz radio polarimeter at Nobeyama Radio Observatory, while the flare locations have been identified from X-ray flare lists maintained by NOAA/SEL. Only those flares showing more than 10 sfu of circularly polarized flux at 17 GHz are plotted. The radius of the circle for each event is a logarithmic measure of the magnitude of the circularly polarized flux: open circles indicate "negative" or left-handed circular polarization, normally corresponding to downgoing magnetic fields, while filled circles denote "positive" or right-handed circular polarization, normally corresponding to upgoing magnetic fields.

Figure 5 shows variations on the timescales both of the solar cycle and of solar rotation. The solar rotation variation is due to bright regions rotating on and off the disk: at frequencies in the 1 - 10 GHz range where the quiet Sun corona is optically thin but active regions can be optically thick, a large area at coronal brightness temperature can make a large difference to the Sun's radio flux, changing it by up to 100%. This effect is most visible at the lower frequencies. The yearly modulation due to the variation in the Earth's distance from the Sun is also apparent. Schmahl & Kundu (1997) have discussed the solar cycle variation of the solar radio spectrum and its causes in detail, while Zirin, Baumert & Hurford (1991) have analyzed the radio brightness temperature spectrum of the quiet Sun atmosphere.

Inspection of Figure 5 suggests that, viewed as a distant star, the Sun's radio emission could reveal the solar cycle at the lower frequencies but only if sufficiently intense monitoring were carried out: sporadic observations carried out once or twice a year over the solar cycle may not show a clear pattern due to the confusing effects of modulation on the rotation timescale and of flares (absent from Figure 5).

Another tracer of the solar cycle is the inversion of the dominant polarity in each hemisphere that accompanies new cycles. The clearest signature of this effect is in the east-west orientation of the polarity of photospheric magnetic fields: solar active

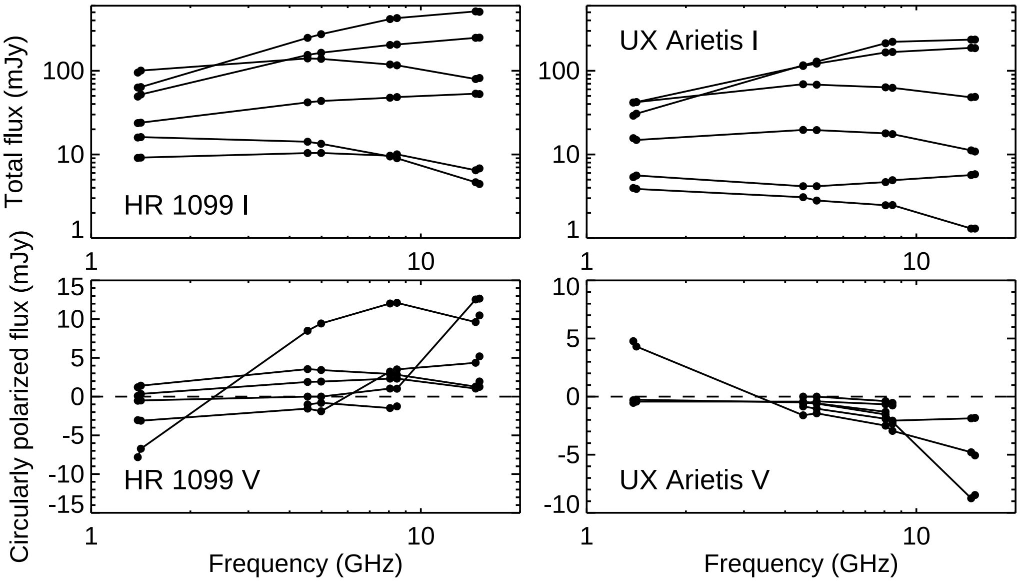

Figure 7. A sample of radio flux measurements for two RS CVn systems, HR 1099 (left panels) and UX Arietis (right panels). The upper panels show flux spectra from 1.4 to 15 GHz measured with the Very Large Array on 6 different dates from 1993 to 2000, while the lower panels show the corresponding circularly polarized flux spectra. High flux states correspond to episodes of flaring when polarization tends to be low (Mutel et al. 1987).

regions tend to have large leading spots at their western (leading) edge, trailed by a collection of smaller spots of opposite magnetic polarity. The polarity of the leading spot is a function of the hemisphere in which it is located and the solar cycle. In the current cycle (cycle 23), leading spots in the northern hemisphere are usually of "positive" or upgoing magnetic polarity, while leading spots in the southern hemisphere are "negative" or downgoing polarity. As noted earlier, radio observations of the sense of circular polarization reflect the orientation of the magnetic field in the source, and it is appropriate to ask whether we see the solar cycle reflected in the radio polarization. Figure 6 shows measurements of the sense of circular polarization at 17 GHz as a function of position on the Sun for 59 flares in cycle 22 (1990-1995) and 99 flares in cycle 23 (1997-2001). While the statistics here are not as good as one would like, the figures do establish that the polarization of the high-frequency gyrosynchrotron emission in a given hemisphere varies from flare to flare. There is a predominance of "positive" (right-handed) circular polarization in the northern hemisphere in cycle 23 and "negative" (left-handed) circular polarization in the southern hemisphere, as expected from the leading spot analogy, but a given event in either hemisphere can show either polarization. This is consistent with the fact that a flare can occur anywhere in an active region and its circular polarization will reflect the local polarity of the magnetic field rather than the large-scale polarity of the active region.

This result makes the analogous observation for active stars even more puzzling. In the early days of stellar radio astronomy Dave Gibson (1983) noted, based on the limited sample of data then available, that a given active star tended to show the same sense of circular polarization in its radio emission every time it was observed. This observation continues to hold true but with a much greater wealth of data to support it. Figure 7 shows some examples of radio spectra in both total flux and circularly polarized flux for two well-known RS CVn stars, HR 1099 and UX Arietis. Gibson noted in 1983 that HR 1099 is always right circularly polarized and that UX Ari is always left circularly polarized. Ignoring the lower frequencies (where plasma emission, which has a sense of polarization opposite to that of gyrosynchrotron emission, tends to dominate the polarization; White & Franciosini 1995), we see that HR 1099 continues always to show positive circular polarization at the higher frequencies while UX Ari continues to show negative circular polarization roughly 30 years since the first measurements (the figure shows only a small fraction of the available data). This constancy in the sense of circular polarization is also true of those dwarf, pre-main-sequence and magnetic B stars that have been detected as sources of circularly-polarized radio emission, whether flaring or quiescent. Comparing the radio flux spectra in Figures 6 & 7, we also see that active stars have radio spectra flatter than those of solar flares and without the pronounced peak that is usually observed in solar flare spectra.

Gibson (1983) noted that from the Earth our view of HR 1099 and UX Ari is dominated by a single hemisphere because of their orientation, and argued that a feature analogous to the leading spot property of solar active regions might explain the steady sense of circular polarization. The orientation of the magnetic field in stellar spots can also be determined from Zeeman Doppler imaging. It has been argued that by searching for reversals in these fields we can detect stellar cycles (e.g., Donati et al. 1992), for the few stars bright enough and rotating rapidly enough that the difficult technique of Zeeman Doppler imaging can be employed. Radio observations offer a simple complement to this approach, and the chance to extend the search to a broader range of stars than can be studied with Zeeman Doppler imaging, since we can detect circular polarization in the radio emission of many classes of stars (main–sequence dwarfs from F to M class, cool subgiants, and G–M pre–main–sequence stars). However, our observations to date have failed to show a clear example of a polarization reversal in any active star, implying activity cycles of at least 40 years.

Acknowledgments. Support for the preparation of this material was provided by NSF grant ATM 99-90809 and NASA grant NAG 5-8192. We thank the Nobeyama Radio Observatory for making their excellent data readily available.

References

Bastian, T. S., Benz, A. O., & Gary, D. E. 1998, ARA&A, 36, 131

Bastian, T. S., Pick, M., Kerdraon, A., Maia, D., & Vourlidas, A. 2001, ApJ, 558, L65

Benz, A. O., & Güdel, M. 1994, A&A, 285, 621

Donati, J., Brown, S. F., Semel, M., Rees, D. E., Dempsey, R. C., Matthews, J. M., Henry, G. W., & Hall, D. S. 1992, A&A, 265, 682

Dulk, G. A. 1985, ARA&A, 23, 169

Gibson, D. M. 1983, in Cool Stars, Stellar Systems and the Sun, ed. S. L. Baliunas & L. Hartmann (Berlin: Springer Verlag), p. 197

Güdel, M., & Benz, A. O. 1993, ApJ, 405, L63

Güdel, M., Schmitt, J. H. M. M., Bookbinder, J. A., & Fleming, T. A. 1993, ApJ, 415, 236

Lee, J., White, S. M., Gopalswamy, N., & Kundu, M. R. 1997, Solar Phys., 174, 175

Mutel, R. L., Morris, D. H., Doiron, D. J., & Lestrade, J. F. 1987, AJ, 93, 1220

Nakajima, H., and 8 others. 1985, PASJ, 37, 163

Nindos, A., White, S. M., Kundu, M. R., & Gary, D. E. 2000, ApJ, 527, 415

Schmahl, E. J., & Kundu, M. R. 1998, in Synoptic Solar Physics, ed. K. S. Balasubramaniam, J. W. Harvey, & D. Rabin (San Francisco: Astron. Soc. Pacific (Conf. Ser. 140)), p. 387

Torii, C., Tsukiji, Y., Kobayashi, S., Yoshimi, N., Tanaka, H., & Enome, S. 1979, Proc. Nagoya Univ. Research Inst. of Atmospherics, 26, 129

White, S. M. 1996, in Cool Stars, Stellar Systems and the Sun (9th Conference), ed. R. Pallavicini & A. K. Dupree (San Francisco: PASP), p. 21

White, S. M., & Franciosini, E. 1995, ApJ, 444, 342

White, S. M., & Kundu, M. R. 1997, Solar Phys., 174, 31

Zirin, H., Baumert, B. M., & Hurford, G. J. 1991, ApJ, 370, 779

Zlotnik, E. Y. 1968, Sov. Astron., 12, 245